Spectral Analysis of Numerical Error of Methods in Two-Dimensional Heat Diffusion

Luke Engstrom,[1,*] Jason Fan,[1,†] Chad Smith,[1,‡] Alexander Nava,[1,§] and Ahan Sarkar[1,¶]

[1] *Department of Physics, University of California, Berkeley*

(Dated: April 13, 2026)

Primarily using the two-dimensional heat equation in conjunction with explicit and implicit methods to model heat diffusion, we show that there are key limitations to each approach, with a primary focus on the implicit model. To obtain these results, we vary several components of the heat equation, including the diffusivity constant and the time step size, and for a more rigorous analysis of the implicit method, a phase angle θ as well. We use the Peaceman–Rachford method and the Alternating Direction Implicit (ADI) scheme with Fourier-based techniques. From this, we identify the explicit CFL limit beyond which FTCS diverges, and we show that the ADI method, while unconditionally stable, demonstrates direction-dependent error. This directional error grows with timestep size and is accentuated for particular complex phases θ when we analytically continue the diffusivity into the complex plane. Understanding these limitations is important for evaluating the effectiveness of the heat equation in computational modeling, as it is widely used across many fields.

I. INTRODUCTION AND PHYSICS MOTIVATION

In this paper we investigate the numerical stability and accuracy of explicit and implicit methods for solving the two-dimensional heat equation in contexts where systems are vulnerable to overheating. Using the forward Euler method for the explicit scheme and the Peaceman–Rachford Alternating Direction Implicit (ADI) method for the implicit scheme, we simulate heat diffusion under varying time steps, diffusivity values, and complex phase angles. Stability is assessed through comparison with analytical stability conditions, while accuracy is evaluated by comparing numerical solutions to the analytical Gaussian solution.

Among standard numerical approaches, explicit finite-difference schemes such as Forward Time Centered Space (FTCS) are simple to implement but subject to a strict CFL stability constraint (Fig. 1). Implicit schemes remove the timestep restriction; however, a fully implicit 2D Crank–Nicolson update requires solving a large coupled linear system. Alternating Direction Implicit (ADI) factorizations (for example the Peaceman–Rachford variant) address this cost by splitting the 2D update into two sequential 1D implicit solves per time step, at the expense of operator-splitting error. This paper studies the trade-off between unconditional stability and the anisotropic accuracy consequences of that splitting.

The computational techniques matter because in real-world systems that depend on heat, it is often best to simulate the situation before experimentation and implementation as these types of systems pose extreme and avoidable risks. Additionally, computational methods are

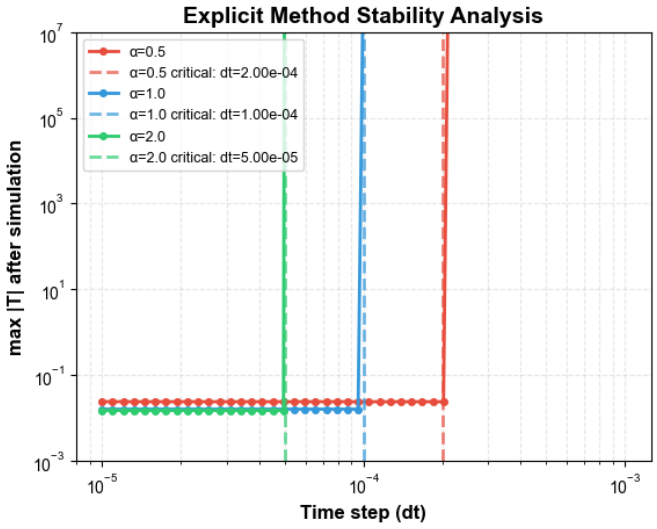

FIG. 1. **Stability Analysis.** Model stability plots showing the max temperature of simulations for both explicit and implicit models and whether each simulation was stable or unstable.

crucial as analytical ones often fail to capture the complexity of heat diffusion [1]. The computational approach also allows researchers to assess stability, error, and appropriate time steps to ensure the safety and efficacy of the system under study.

The motivation and physical context is that modeling heat diffusion is critical for systems where thermal management is a safety constraint, such as in microprocessors, aerospace thermal protection, and nuclear reactor cores. In these contexts, analytical methods often fail to capture complex geometries [1], necessitating robust computational approaches.

A prime example is the thermal stability of Pressurized Water Reactors (PWRs). In a reactor core, heat generated by fission must be continuously removed to prevent fuel rod melting. During transient events like a loss-of-coolant accident (LOCA), the timescale of heat conduc-

* luke.engstrom@berkeley.edu
† jasonfan@berkeley.edu
‡ chad.smith@berkeley.edu
§ alexander_nava@berkeley.edu
¶ ahansarkar@berkeley.edu

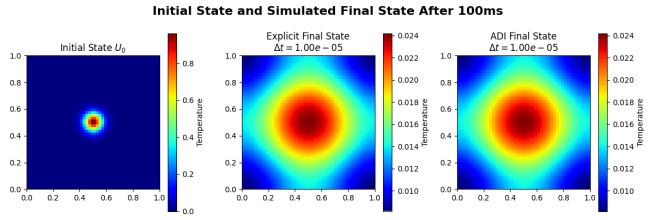

FIG. 2. **Example Stability Simulations.** Temperature plots show the initial conditions of the grid for each simulation and an example simulation of each numerical solver with $\alpha = 0.5$ and $dt = 10^{-5}$.

tion determines safety margins. This scenario models a diffusion problem where the temperature field $u(x,t)$ evolves according to:

$$\frac{\partial u}{\partial t} = \nabla \cdot (\alpha(x)\nabla u) + Q(x,t)$$

In these high-stakes simulations, numerical stability is crucial. Explicit methods can fail catastrophically if the time step exceeds the stability limit ($\Delta t \propto h^2/\alpha$), creating a risk of non-physical "blow-ups" in safety models. Consequently, unconditionally stable schemes like the Alternating Direction Implicit (ADI) method are the standard for these applications.

However, stability does not guarantee accuracy. The operator splitting used in ADI introduces subtle artifacts, such as directional bias (anisotropy) and non-physical decay rates for high-frequency modes. This paper accepts ADI as the necessary tool for stability but rigorously investigates its accuracy limitations, specifically analyzing the spectral and directional errors that arise when using large time steps in critical diffusion models.

While the ADI method offers unconditional stability, it introduces a specific accuracy limitation known as *splitting error*. In the continuous limit, the spatial derivatives ∂_x^2 and ∂_y^2 commute; however, the numerical factorization of the 2D evolution operator into sequential 1D sweeps is only exact if the discrete operators D_{xx} and D_{yy} commute perfectly. According to the Baker–Campbell–Hausdorff formula, this introduces a splitting error proportional to the commutator of the operators in shape of Error $\propto \frac{(\Delta t)^2}{2}[D_{xx}, D_{yy}] + \mathcal{O}(\Delta t^3)$, where $[D_{xx}, D_{yy}] = D_{xx}D_{yy} - D_{yy}D_{xx}$. This term implies that the numerical solution is not isotropic but the error depends on the order of operations (x-first vs. y-first). Consequently, we expect the numerical fidelity to degrade along specific axes where this commutation error is maximized, a hypothesis we test by analyzing the solution's spectral behavior in the complex plane.

Contributions

- Implemented and validated explicit FTCS and implicit Peaceman-Rachford ADI schemes for the 2D heat equation.
- Demonstrated classical stability limits for explicit schemes and unconditional stability for ADI.
- Quantified ADI accuracy limitations using Fourier-space analysis, angular (directional) error evaluation, and temporal convergence studies.
- Extended the ADI solver to three dimensions and explored computational performance.
- Provided fully reproducible code and simulation notebooks, enabling replication of all results and figures.

Paper Road Map

First, we introduce the key equations and background information necessary to understand the numerical methods used in this work. Next, we explain how these mathematical methods are implemented computationally and what they represent physically. We then demonstrate how the methods are applied in practice and present our results. Finally, we discuss the limitations of the project and outline possible directions for future work.

II. BACKGROUND AND RELATED WORK

2D heat equation:

$$\frac{\partial u}{\partial t} = \alpha(\frac{\partial^2 u}{\partial x^2} + \frac{\partial^2 u}{\partial y^2})$$

Here, $u(x,y,t)$ represents the temperature field, α is the thermal diffusivity constant, and x and y are spatial coordinates. This equation describes heat flow within a system under the assumption of a constant diffusivity throughout the domain. Because of the complexity of real-world systems, this equation alone is often insufficient to describe realistic heat diffusion, and numerical methods are required to obtain practical solutions. In this project, we focus on discrete spatial grids combined with implicit time-stepping schemes.

Prior studies have analyzed the stability and convergence of finite-difference schemes for partial differential equations, including explicit Euler methods, Peaceman–Rachford schemes, and ADI factorizations [1–6].

Implicit time-stepping and operator splitting. Implicit schemes such as the Peaceman–Rachford method provide unconditional stability for parabolic equations like heat diffusion. In two spatial dimensions, however, a fully implicit Peaceman–Rachford update requires solving a large coupled linear system involving all grid points. To reduce computational cost, Alternating Direction Implicit (ADI) schemes are commonly used, in which the two-dimensional operator is split into a sequence of one-dimensional implicit solves. In this work, Peaceman–Rachford ADI is used as the primary implicit method

for stability and accuracy analysis, while a Peaceman–Rachford ADI variant is employed selectively in the nuclear reactor simulation for computational efficiency.

Utilizing complex values of α to analyze anisotropy. To test the anisotropy of the ADI model, we decided to explore what would occur when the diffusivity is moved into the complex plane by rotating it by a complex phase angle θ. This approach is not meant to reflect any real physical system but rather serves as a mathematical tool for exploring the behavior of the numerical method. Complex analysis is necessary since fourier mode decay depends only on scalar values, thus by introducing anisotropy via the ADI scheme, we also introduce error. Let the diffusivity be continued into the complex plane, writing either

$$\alpha = \alpha_r + i\,\alpha_i, \qquad \text{or equivalently} \qquad \alpha = |\alpha| e^{i\theta},$$

so that $\theta = \arg(\alpha)$ is the phase of the complex diffusivity. The governing heat equation from earlier remains formally unchanged, but the resulting value depends on the phase angle θ at which it is rotated in that respective direction. This allows us to evaluate error with respect to α, as α rotates around the complex plane. To cover both cases, we analyze the error with X-first and Y-first splitting ADI.

III. DATA AND EXPERIMENTAL/SIMULATION SETUP

Simulation Conditions

All simulations use a uniform, Cartesian grid with N points per side. For experiments that employ FFT-based spectral comparisons (Sections IV and V) we use a periodic grid with coordinates

$$x_i = i\frac{L}{N}, \quad i = 0, \ldots, N-1,$$

so the grid spacing is $h = L/N$ and the discrete Fourier wavenumbers are generated with `fftshift(fftfreq(N, d=L/N)) * 2*pi`. For non-periodic experiments (Neumann/Dirichlet boundary tests) we use $x \in [0, L]$ with $x_i = iL/(N-1)$ and $h = L/(N-1)$. The initial condition (except FFT simulation) was taken to be a smooth two–dimensional Gaussian,

$$u(x, y, 0) = \exp\left(-\frac{(x-x_0)^2 + (y-y_0)^2}{\sigma^2}\right),$$

Reflective (Neumann-like) boundary conditions were imposed via edge padding. The solution was evolved to a fixed final time T. For calculations of accuracy comparing to analytical solution of the gaussian distribution the relative L_2 error was computed as

$$\varepsilon(\Delta t) = \frac{\|u_{\Delta t}(T) - u_{\text{ref}}(T)\|_2}{\|u_{\text{ref}}(T)\|_2}.$$

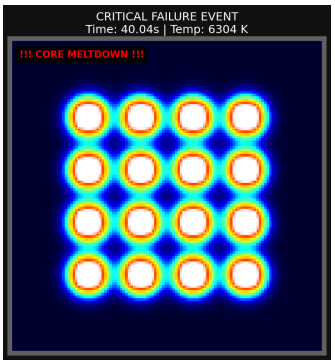

FIG. 3. Simulation of when nuclear power plants reach critical failure due to excessive heat.

A. Simulation Setup: Reactor Core LOCA Model

To simulate a loss-of-coolant accident (LOCA), the two-dimensional diffusion equation was solved on a 1.0 m $\times$ 1.0 m domain discretized into a 120×120 uniform grid. The reactor core geometry was modeled as a 4×4 lattice of square fuel rods embedded in a moderator matrix. Material heterogeneity was incorporated via a spatially varying diffusivity $\alpha(\mathbf{x})$, where $\alpha_{\text{fuel}} = 1.0 \times 10^{-4}\,\text{m}^2\,\text{s}^{-1}$ and $\alpha_{\text{mod}} = 2.0 \times 10^{-5}\,\text{m}^2\,\text{s}^{-1}$.

The system was initialized at 300 K subject to a constant volumetric heat source of $\sim 800\,\text{K}\,\text{s}^{-1}$ within the fuel regions. Active cooling was modeled by enforcing fixed Dirichlet boundary conditions ($u|_{\partial\Omega} = 300\,\text{K}$) for the first 40 s, allowing the system to reach a steady operating temperature of approximately 600 K. At $t = 40\,\text{s}$, the boundary conditions were relaxed to simulate total coolant pump failure, driving the system toward the zirconium cladding melting point (2100 K) and subsequent fuel meltdown.

IV. METHODS

Computational pipeline. Simulations begin by initializing a two-dimensional uniform grid with a Gaussian temperature profile. For each time step, the temperature field is evolved using the implicit Peaceman–Rachford ADI method. Boundary conditions are applied at each update, and the solution is advanced until a fixed final simulation time is reached. Stability is assessed by monitoring the maximum temperature, while accuracy is evaluated by comparing the numerical solution to the analytical Gaussian solution. For spectral analysis, a two-dimensional Fourier transform of the temperature field is computed, and the decay of implicit method is compared against the exact exponential decay predicted by the heat equation.

Numerical/ML methods. We employ two numerical approaches: an explicit Forward Time Centered-Space (FTCS) scheme and an implicit Peaceman–Rachford

method implemented using Alternating Direction Implicit (ADI) splitting.

Key equations. For Peaceman–Rachford ADI method, the simulation solves the two-dimensional heat equation

$$u_t = \alpha(u_{xx} + u_{yy})$$

on a unit square. A uniform grid (x_i, y_j) on a domain of length L with N points per side is used. For periodic spectral tests we take $h = L/N$; for non-periodic tests we use $h = L/(N-1)$. Second-order central differences approximate spatial derivatives.

$$u_{xx}(i,j) \approx \frac{u_{i+1,j} - 2u_{i,j} + u_{i-1,j}}{h^2},$$
$$u_{yy}(i,j) \approx \frac{u_{i,j+1} - 2u_{i,j} + u_{i,j-1}}{h^2}.$$

Physically, this measures how the solution curves in horizontal (x) and vertical (y) directions by comparing each value to its immediate left and right neighbors.

Then, let dt be the time step, and define

$$k = \frac{\alpha\, dt}{2h^2}.$$

Each time step is split into two half-steps: Y-implicit and X-implicit. For Y-implicit, we have

$$(I - kD_{yy})u^* = (I + kD_{xx})u^n$$

where D_{yy} is the 1-D second-difference operator acting along the y-direction. This is applied independently to each row; the matrix $(I - kD_{yy})$ is tridiagonal.

For X-implicit half-step,

$$(I - kD_{xx})u^{n+1} = u^* + kD_{xx}u^*,$$

where D_{xx} is the 1-D second-difference operator in the x-direction. This is applied independently to each column.

The explicit Forward Time Centered-Space (FTCS) method solves the same two-dimensional heat equation

$$u_t = \alpha(u_{xx} + u_{yy})$$

uniform grid (x_i, y_j) on a domain of length L with N points per side is used.

Second-order central differences approximate the spatial derivatives:

$$u_{xx}(i,j) \approx \frac{u_{i+1,j} - 2u_{i,j} + u_{i-1,j}}{h^2},$$
$$u_{yy}(i,j) \approx \frac{u_{i,j+1} - 2u_{i,j} + u_{i,j-1}}{h^2}.$$

Physically, these expressions measure the curvature of the temperature distribution in the horizontal and vertical directions by comparing each grid point to its four nearest neighbors.

All FFT-based spectral analyses were performed under periodic boundary conditions in both spatial directions. For these experiments, the ADI solver was configured with wrap-around (periodic) boundary handling so that discrete Fourier modes are exact eigenfunctions of the numerical Laplacian. This assumption is required for the analytical Fourier-space propagator $\exp\left[-\alpha(k_x^2 + k_y^2)t\right]$ to be a valid reference. Spectral comparisons are therefore restricted to simulations using periodic boundaries; results obtained with reflective (Neumann-like) padding are excluded from the FFT fidelity analysis.

Time Discretization

The time derivative uses the forward Euler approximation:

$$u_t(i,j,t^n) \approx \frac{u_{i,j}^{n+1} - u_{i,j}^n}{\Delta t}.$$

Substituting this and the spatial differences into the heat equation gives

$$\frac{u_{i,j}^{n+1} - u_{i,j}^n}{\Delta t}. = \alpha\Bigg(\frac{u_{i+1,j}^n - 2u_{i,j}^n + u_{i-1,j}^n}{h^2} + \frac{u_{i,j+1}^n - 2u_{i,j}^n + u_{i,j-1}^n}{h^2}\Bigg)$$

Define the dimensionless time step ratio

$$r = \frac{\alpha\,\Delta t}{h^2}.$$

Explicit Update Formula

Solving for $u_{i,j}^{n+1}$ yields the FTCS update:

$$u_{i,j}^{n+1} = u_{i,j}^n + r\left(u_{i+1,j}^n + u_{i-1,j}^n + u_{i,j+1}^n + u_{i,j-1}^n - 4u_{i,j}^n\right).$$

This update requires only values from the previous time step; no linear system is solved.

Physical Interpretation

The term

$$u_{i+1,j}^n + u_{i-1,j}^n + u_{i,j+1}^n + u_{i,j-1}^n - 4u_{i,j}^n$$

is the discrete 5-point Laplacian, which measures how much $u_{i,j}$ differs from the average of its neighbors. A point hotter than its surroundings decreases, while a cooler point increases, reflecting diffusion.

Stability Condition

Von Neumann analysis shows that FTCS is stable only if

$$r_x + r_y \leq \frac{1}{2}.$$

For equal grid spacing in x and y ($h_x = h_y = h = \frac{L}{N-1}$), this reduces to

$$r = \frac{\alpha\,\Delta t}{h^2} \leq \frac{1}{4}.$$

If this condition is violated, at least one Fourier mode satisfies $|G| > 1$, and the numerical solution will diverge.

Fast Fourier Transform

Transforming the heat equation $\frac{\partial u}{\partial t} = \alpha \nabla^2 u$ into Fourier space yields a system of decoupled ordinary differential equations for each wavenumber k:

$$\frac{\partial \hat{u}(k,t)}{\partial t} = -\alpha |k|^2 \hat{u}(k,t)$$

At the same time, the exact analytical solution for a given Fourier mode at time t is:

$$\hat{u}_{\text{exact}}(k,t) = \hat{u}_0(k) \cdot e^{-\alpha(k_x^2+k_y^2)t}$$

In the numerical implementation using Fast Fourier Transforms (FFT), the wavenumbers are discretized based on the domain length L and the number of grid points N. For indices $m, n \in [-\frac{N}{2}, \frac{N}{2} - 1]$:

$$k_x = \frac{2\pi m}{L}, \quad k_y = \frac{2\pi n}{L}$$

and $|k|^2 = k_x^2 + k_y^2$ represents the square of the wavenumber magnitude.

To evaluate the accuracy of the ADI scheme, we compute the ratio of the numerical solution's spectral amplitude to the exact analytical amplitude. Let $\hat{u}_{\text{num}}$ be the FFT of the result from the numerical solver, then the fidelity metric R is defined as:

$$R(k) = \frac{|\hat{u}_{\text{num}}(k,t)|}{|\hat{u}_{\text{exact}}(k,t)|}.$$

Code snippet. To implement this method numerically, we used the ADI scheme, in which each timestep is split into two directions, in this case x and y corresponding to the horizontal and vertical. In one direction the update is calculated implicitly, while the other direction is done explicitly, and then the methods for the directions alternate in the second half-step.

Listing 1. Implicit Method

```
for it in range(max_iter-1):

    # Explicit y-direction Laplacian
    u_padded = np.pad(u, 1, mode='edge')
    U_y_plus = u_padded[1:-1, 2:] # u[i, j+1]
    U_y_minus = u_padded[1:-1, 0:-2] # u[i, j-1]
    RHS1 = u + k * (U_y_minus - 2.0*u + U_y_plus)

    u_star = np.linalg.solve(A, RHS1)

    # Explicit x-direction Laplacian
    u_padded = np.pad(u_star, 1, mode='edge')
    U_x_plus = u_padded[2:, 1:-1] # u[i+1, j]
    U_x_minus = u_padded[0:-2, 1:-1] # u[i-1, j]
    RHS2 = u_star + k * (U_x_minus - 2.0*u_star +
        U_x_plus)

    u = np.linalg.solve(C, RHS2.T).T

    u_pred.append(np.copy(u))
```

Peaceman–Rachford ADI Method in the Reactor Simulation

For the nuclear reactor simulation, the Peaceman–Rachford ADI method is implemented using the Peaceman–Rachford formulation. This choice is motivated by computational considerations rather than analytical necessity: the reactor model requires large spatial grids and long simulation times, for which solving fully coupled implicit systems becomes prohibitively expensive.

The Peaceman–Rachford scheme is a specific ADI factorization of the Peaceman–Rachford method, in which the two-dimensional Laplacian is split into sequential one-dimensional operators. Advancing the solution from time step n to $n+1$ proceeds through an intermediate state u^*:

$$(I - kD_{xx})\,u^* = (I + kD_{yy})\,u^n, \tag{1}$$

$$(I - kD_{yy})\,u^{n+1} = (I + kD_{xx})\,u^*, \tag{2}$$

where $k = \frac{\alpha \Delta t}{2h^2}$.

This formulation preserves the unconditional stability of Peaceman–Rachford while reducing each implicit solve to a set of independent tridiagonal systems.

V. RESULTS

A. Result I: Baseline Accuracy Analysis

With the analytical solution for the Gaussian initial condition, both numerical models can be compared in their accuracy based on how closely they mimic the analytical solution. (Fig. 4) compares this error for both ex-

plicit and implicit models across various time steps that were all small enough to not diverge.

The explicit method appears to be consistent in accuracy for sufficiently small values of Δt but near the stability limit it becomes more inaccurate.

The implicit method, however, shows a non-monotonic error minimum at a higher value of Δt before eventually converging back to the accuracy of very small values. The accuracy analysis indicates that the two methods have similar behavior in error creation but that the implicit method maintains accuracy over a wider range of stable time steps than the explicit scheme for this diffusion problem.

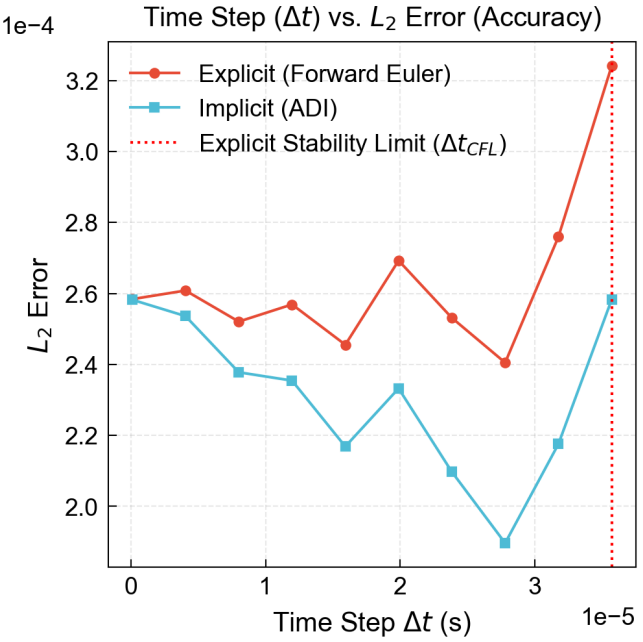

FIG. 4. **Result I: Numerical Model Error vs. Time Step Size.** Simulation error plots showing the L2 error of the final state of simulations of different time steps from 10^{-7} to 3.5×10^{-7} compared to ground truth (analytical solution).

B. Result II: FFT Analysis

To assess how our ADI scheme models the spectral decay of diffusion, we also compared the simulation with an FFT solution to heat diffusion.

Using a square domain with grid size $N = 100$ and $\alpha = 1.0$ the spectral accuracy of the model was evaluated by comparing the ADI solution at each mode with the exact FFT solution given by

$$\hat{u}(k_x, k_y, t) = \hat{u}(k_x, k_y, 0)\, e^{-\alpha\left(k_x^2 + k_y^2\right)t}$$

The ratios of amplitudes calculated by the ADI model and FFT solution are plotted in (Fig. 5) with the mean for each binned wavenumber magnitude $|k|$ plotted in a line.

This simulation showed that at low wavenumbers the ADI model accurately reflects ideal dissipation. At higher wavenumbers, increased scatter from ideal physics is observed, deviations from ideal exponential decay consistent with numerical dispersion or splitting error.

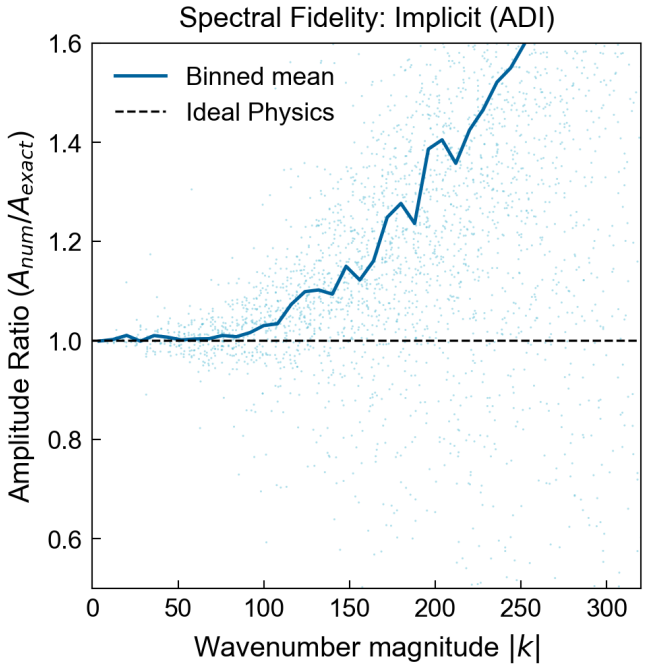

FIG. 5. **Result II: Amplitude Ratio vs. Fourier Mode.** Plot showing the spectral fidelity of an implicit ADI diffusion solver by directly comparing numerical and exact Fourier-mode decay ratios and averaging ratios at each mode.

C. Result III: Complex α and Anisotropy of the ADI Scheme

The ADI method is not exact, using a factorization of the Laplacian as described in **IV**. This gives rise to the error in the simulations. Since the simulation works in two spatial dimensions, it uses two second-derivative operators and the sweep order determines which way it splits first.

The ADI scheme can be written in two sweep orders:

XY order:

$$(I - kD_x)\, u^* = (I + kD_y)\, u^n,$$
$$(I - kD_y)\, u^{n+1} = (I + kD_x)\, u^*.$$

YX order:

$$(I - kD_y)\, u^* = (I + kD_x)\, u^n,$$
$$(I - kD_x)\, u^{n+1} = (I + kD_y)\, u^*.$$

Here, D_x and D_y are the discrete second-derivative operators in the x and y directions, respectively.

To test the anisotropy of the ADI model, we decided to explore what would occur when the diffusivity is moved into the complex plane by rotating it by a complex phase angle θ. This approach is not meant to reflect any real physical system but rather serves as a mathematical tool for exploring the behavior of the numerical method.

The error plots for simulation starting with splitting in the X direction (Fig. 6) and Y direction (Fig. 7) spike at the angles corresponding to Fourier modes aligned with the direction treated implicitly in the first ADI sweep. This reflects a directional bias introduced by the operator splitting: because the diffusion operator is factorized into sequential one-dimensional solves, modes aligned with the first sweep direction experience different numerical damping than modes aligned with the orthogonal direction. As a result, the numerical error depends on the orientation of the mode relative to the sweep order.

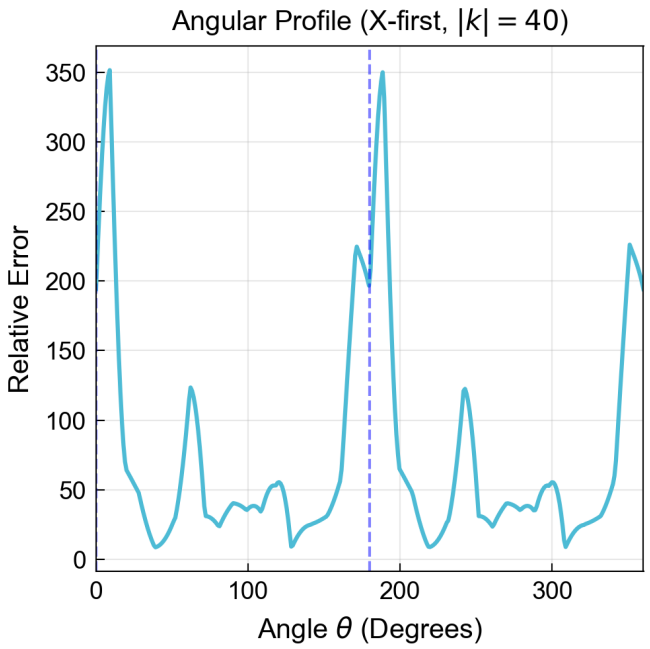

FIG. 6. **Result III: Theta Error Analysis (x First).** From this we can see that in the x direction rotation the error is most prominent near 0 degrees and near 180 degrees.

D. Result IV: Temporal Convergence of the ADI Scheme

To quantify the temporal accuracy of the alternating–direction implicit (ADI) method, we performed a systematic convergence study with respect to the time step size Δt. The spatial grid and initial condition were held fixed, and a high–resolution reference solution was computed using the same ADI scheme with a sufficiently small time step Δt_{ref}.

A sequence of simulations was performed with decreasing time step sizes Δt, while keeping the spatial discretization unchanged. The resulting errors were fit to a power law of the form

$$\varepsilon(\Delta t) \propto \Delta t^{\,p},$$

allowing the effective temporal order of accuracy p to be estimated from a linear fit in log–log space. The measured convergence rate was approximately $p \approx 1.1$ (Tab. I), indicating sub–quadratic temporal accuracy. Although local slopes over limited ranges appear consistent with second-order behavior, the global fit is dominated by first-order splitting error, indicating that the asymptotic second-order regime was not reached for the time steps studied. For finite time steps, the splitting error contributes an $O(\Delta t)$ component that dominates the global error before the asymptotic second–order regime is reached.

This result demonstrates that unconditional stability of the ADI method does not guarantee second–order accuracy in practical regimes, particularly when relatively large time steps are employed. The convergence behavior observed here is consistent with the anisotropic and direction-dependent errors identified in the Fourier-space and angular analyses presented in subsequent sections.

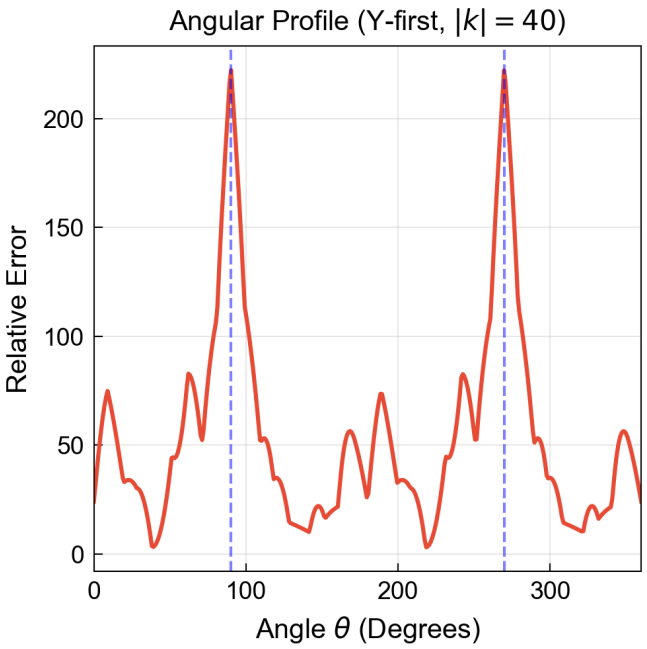

FIG. 7. **Result III: Theta Error Analysis (y First).** From this we can see that in the y direction rotation the error is most prominent near 90 degrees and near 270 degrees.

E. Result V: Extension into the third dimension

While most of our analysis stemmed from two-dimensional scenarios, most thermal systems function in three dimensions. The prior heat equation no longer functions and a new one must be used.

TABLE I. **Result IV: ADI Convergence Study**

Δt	CFL factor	Steps	L_2 error	Max angular error	Anisotropy
1.00×10^{-6}	0.0	2000	1.59×10^{-8}	5.35×10^{-7}	3.91×10^{-7}
2.00×10^{-6}	0.1	1000	7.97×10^{-8}	2.68×10^{-6}	1.95×10^{-6}
4.00×10^{-6}	0.2	500	3.35×10^{-7}	1.12×10^{-5}	8.21×10^{-6}
1.00×10^{-5}	0.4	200	2.12×10^{-6}	7.12×10^{-5}	5.20×10^{-5}
2.00×10^{-5}	0.8	100	8.49×10^{-6}	2.85×10^{-4}	2.08×10^{-4}
4.00×10^{-5}	1.6	50	3.40×10^{-5}	1.14×10^{-3}	8.33×10^{-4}
8.00×10^{-5}	3.2	25	1.36×10^{-4}	4.57×10^{-3}	3.33×10^{-3}
1.25×10^{-4}	5.0	16	3.32×10^{-4}	1.12×10^{-2}	8.14×10^{-3}

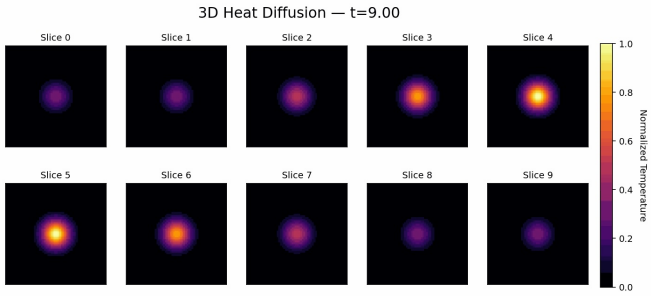

FIG. 8. **Result V: Three Dimensional Heat Diffusion.** A snapshot 10 vertical slices of a cube with an initially heated core spreading heat over time.

$3D$ heat equation:

$$u_t = \alpha(u_{xx} + u_{yy} + u_{zz})$$

Additionally, instead of an $N \times N$ grid it will be simulated in a $N \times N \times N$ grid. Meanwhile the methods will remain linearly the same except applied in an extra dimension, so the ADI for example will take into account the x, y and now z directions.

Figures. Choose 2–4 plots that tell the story (label axes with units; readable legends). Cite the relevant figures in the texts (Fig. 8)

VI. DISCUSSIONS

Validations. The numerical solvers were compared to known analytical results for the heat equation. In particular, simulations with a Gaussian temperature profile were compared to the exact analytical Gaussian solution, and Fourier-mode decay rates were compared to the expected exponential decay. Validation came from ensuring that before non-physical results were observed the analytical and the numerical values mostly agreed.

Uncertainty. The discretization of space and time is the primary source of error, rather than observational uncertainty. This was assessed by varying the time step and observing the resulting numerical error.

Ablations. The most important settings for the explicit method were the time step size and the diffusivity constant as for certain values of each the method would reach non-realistic values. Whereas the implicit method fails at specific θ values in the imaginary plane. While the size of the screen used to simulate and the number of cells in said screen affect the run time.

Limitations. The approach used primarily focused on two-dimensional cases while many real-world applications require three spatial dimensions. Additionally, only conduction with no air flow is considered which are ideal cases and don't mimic scenarios perfectly

VII. COMPUTATIONAL TECHNIQUES, REPRODUCIBILITY, AND CODE AVAILABILITY

Experiments were conducted on a machine running macOS Sequoia, with Python 3.14.0. The following packages were used, with versions specified in `requirements.txt`: `numpy` $\geq$ 1.24.0, `matplotlib` $\geq$ 3.7.0, `scipy` $\geq$ 1.10.0, `pandas` $\geq$ 2.0.0, `sympy` $\geq$ 1.12, `Pillow` $\geq$ 10.0.0, `IPython` $\geq$ 8.12.0, and `FiPy` $\geq$ 3.4.4. Development was performed using Visual Studio Code.

Repository. Public GitHub with README instructions and a Jupyter notebook that directly runs when pulled into Datahub and recreates the results and figures for this report:

- GitHub: https://github.com/Jasonfan06/Physics_77_Heat_Diffusion
- How to run: notebook and/or commands to reproduce figures
- Data access: links or generation scripts, should be in repo

VIII. CONCLUSIONS AND FUTURE WORK

Conclusion. This study characterized the spectral and directional limitations of the Alternating Direction Implicit (ADI) method for the two-dimensional heat equation. While our results confirm the unconditional stability of the Peaceman–Rachford ADI scheme, they also highlight a critical trade-off between stability and isotropic accuracy. Through spectral analysis in the complex diffusivity plane ($\alpha \to |\alpha| e^{i\theta}$), we verified that the operator splitting introduces significant directional bias. Specifically, the Peaceman–Rachford factorization exhibits maximum splitting error at phase angles of $0°, 90°, 180°$, and $270°$.

These error spikes confirm that the splitting error term, proportional to the commutator $[\partial_x^2, \partial_y^2]$, is maximized when transport is aligned with the grid axes. This creates a transient numerical lag in the direction of the initial sweep that degrades the solution for high-frequency modes. Consequently, while ADI is robust against divergence, it introduces artificial anisotropy that must be accounted for in precision-critical thermal modeling.

Future investigations should extend this spectral error analysis to non-rectangular geometries and unstructured meshes. Since the anisotropy observed in this study is inherently linked to the Cartesian grid alignment of the Peaceman–Rachford splitting, applying finite element methods (FEM) on complex domains would determine if such directional biases persist in mesh-independent frameworks.

AUTHOR CONTRIBUTIONS

The following authors contributed to the completion of this project:

- Ahan Sarkar: Stability analysis for rocket and nuclear, spatially variant alpha stability, Nuclear reactor simulation (explicit and implicit).
- Alexander Nava: Rocket simulation (explicit and implicit), $3D$ simulation, Slides creation, Animation creation for error, transformation from explicit to implicit for certain animations, smoothed animation.
- Chad Smith: Derivation of mathematical stability conditions of explicit and implicit methods.
- Jason Fan: Peaceman-Rachford ADI algorithm and animation; Analytical baseline derivation; Spatially varying heat diffusivity algorithm and visualization; Stability algorithm, simulation, and animation; FFT algorithm and graph; spectrum fidelity graph; diffusivity in complex plane derivation, algorithm, and graph; convergence study algorithms.
- Luke Engstrom: Explicit FTCS algorithm, creation of error plots for implicit and explicit, presentation slides, results section, jupyter notebook for all figures.

Refer to the GitHub commit history for details: https://github.com/Jasonfan06/Physics_77_Heat_Diffusion/graphs/contributors.

USE OF AI TOOLS (DISCLOSURE)

AI was used primarily for polishing code and written sections of the report, as well as for guidance in understanding the scope and structure of the project. All numerical methods, simulations, figures, and analysis were developed and verified by the authors.

ACKNOWLEDGMENTS

The authors thank the physics 77/88 staff, especially Harper Sewalls for the guidance and Professor Eric Ma for teaching.

[1] J. Crank, *The Mathematics of Diffusion* (Clarendon Press, 1975).
[2] Y. Pinchover and J. Rubinstein, *An Introduction to Partial Differential Equations* (Cambridge University Press, Cambridge, UK, 2005).
[3] M. Kong, T. Siauw, and A. M. Bayen, *Python Programming and Numerical Methods: A Guide for Engineers and Scientists* (Academic Press, 2020).
[4] K. K. Paudel and H. P. Bhatta, Academic Journal of Mathematics Education **2**, 1 (2023).
[5] J. D. Hunter, Computing in Science & Engineering **9**, 90 (2007).
[6] P. Virtanen *et al.*, Nature Methods **17**, 261 (2020).